IOP Conference Series:
Earth and
Environmental Science

PAPER • OPEN ACCESS

Determination of Hydrodynamic Coefficients for Rotary Derivatives with CFD Simulation

To cite this article: Yuda A. Hermawan *et al* 2025 *IOP Conf. Ser.: Earth Environ. Sci.* **1461** 012037

IOP Conf. Series: Earth and Environmental Science **1461** (2025) 012037 doi:10.1088/1755-1315/1461/1/012037

Determination of Hydrodynamic Coefficients for Rotary Derivatives with CFD Simulation

Yuda A. Hermawan[1*], Ketut Suastika[1], S. Al Farisy[1] and Rizky C. Ariesta[1]

[1] Department of Naval Architecture, ITS Surabaya, 60111 Surabaya, Indonesia

[*]E-mail: yuda.apri@its.ac.id

Abstract. Indonesia possesses rich natural resources, including extensive marine biodiversity and underwater infrastructure. To maximize its potential as a maritime nation, the development of underwater vehicles has emerged as a viable solution. In recent years, there has been significant growth in the development and use of these vehicles, particularly for exploring underwater environments. Hybrid Remotely Operated Vehicles (HROVs) combine the advantages of Autonomous Underwater Vehicles (AUVs) and Remotely Operated Vehicles (ROVs), offering versatile operational modes for industrial applications. UUV Segara Nauta (SN-01) is an HROV developed at the TKD Laboratory of FTK-ITS Surabaya. To ensure effective manoeuvering in various degrees of freedom, the motion abilities of HROVs are evaluated through manoeuver testing, which reveals the vehicle's motion characteristics and response to commands. These characteristics are represented by hydrodynamic coefficients derived from the forces and moments experienced by the vehicle, obtained through CFD numerical simulations. This study performs a virtual captive model test using the UUV Segara Nauta (SN-01) model to conduct rotating arm tests. The focus is on determining the linear hydrodynamic coefficients in the horizontal plane, specifically for sway and yaw motions. Test variations include different drift angles and radius values to assess the effects of lateral and angular velocities. The CFD simulation results, including force and moment values, are converted into non-dimensional values and analyzed using linear regression to obtain the hydrodynamic coefficients. These coefficients explain the model's behavior and underwater hydrodynamic performance, which is more responsive but tends to be unstable.

1. Introduction

The development of Unmanned Underwater Vehicles (UUVs) is crucial for supporting marine biodiversity and underwater infrastructure in Indonesia. To maximize its potential as a maritime nation, Indonesia must focus on developing and constructing its underwater vehicles, emphasizing technical aspects such as hydrodynamic performance, motion, and manoeuvrability. Unlike larger submarines, Unmanned Underwater Vehicles (UUVs) possess unique characteristics. There are various types of UUVs, including Autonomous Underwater Vehicles (AUVs) and Remotely Operated Vehicles (ROVs). However, recent advancements have led to the creation of a new category that combines the advantages of both, known as Hybrid Remotely Operated Vehicles (HROVs). These vehicles vary in size, and the environmental conditions of the water they operate significantly influence the forces and moments exerted on the vehicle's body during impact. These vehicles must maintain operational speeds without harming marine ecosystems and navigate varying depths effectively. Consequently, the vehicle's motion and manoeuvrability are largely determined by its body shape, making it essential to base the vehicle's design on a comprehensive analysis of its manoeuvring performance.

Manoeuvrability is a key factor in determining the limitations of an object's motion and control in water. For an underwater vehicle, manoeuvrability refers to its ability to adjust or maintain speed, depth, direction, and angle of motion, all of which are influenced by the vehicle's control mechanisms [1]. Manoeuvring analysis of underwater vehicles can be conducted using ship manoeuvring methods based on modular mathematical models. These models treat each hydrodynamic component involved in manoeuvring as a separate module, which is then integrated into a comprehensive numerical model for manoeuvring motion [2]. This modular approach allows for easier adjustments and modifications to individual parameters without affecting other components [3]. One such method, the Mathematical Model of Manoeuvring Group, has demonstrated high accuracy in predicting ship manoeuvring behaviour. Applying this modular mathematical model to underwater vehicles is particularly effective for predicting the manoeuvring motion of underwater tourist submarines. However, precise hydrodynamic coefficients are essential to calculate the manoeuvring performance of these vessels accurately.

Manoeuvrability can be evaluated through several methods, including empirical calculations, experimental testing, and numerical simulations. Among these methods, numerical simulation has become a primary approach for assessing the fundamental behaviour and manoeuvrability of a vehicle. Numerical simulations by utilizing computational fluid dynamics (CFD), offering cost-effective, accurate results into hydrodynamic coefficients and motion behaviours, are essential for evaluating UUV performance in six degrees of freedom. These simulations follow standard guidelines and procedures, such as those outlined in the ITTC captive model test procedure. Beyond addressing manoeuvring performance requirements through hydrodynamic coefficients, captive model tests also provide quicker results for assessing compliance with manoeuvring criteria set by IMO regulations. The ITTC procedure offers a detailed, step-by-step approach to simulating standard manoeuvring tests to obtain accurate hydrodynamic coefficients [4]. These coefficients, derived from manoeuvring equations, are crucial for describing and analysing spatial motion in six degrees of freedom (DOF) [5].

In previous studies, various approaches have been undertaken using captive model tests, particularly the rotating arm test. Toxopeus et al. [6] initiated a collaborative study using CFD to perform the calculations of the bare hull DARPA SUBOFF to investigate the capability of viscous-flow solvers for the prediction of the flow field around the hull. Either using static mesh or dynamic mesh, both methods give results that close to each other. Static mesh which non-inertial system is adopted to let the flow rotate around the stationary hull. Cao et al. [7] added source terms to those simulations in order to Coriolis and centrifugal forces will affect water particle to experience due to the rotation of the coordinate system. For different model shapes, Tang et al. [8] analysed the TUNA-SAND AUV, which has a complex block structure resembling a typical ROV, differing from streamlined shapes. They conducted both experimental and numerical simulations to validate their results, focusing on determining 16 viscosity-related damping coefficients and 12 potential flow-related inertia coefficients. Besides that, Hong et al. [9] assessed the hydrodynamic performance of the Underactuated Underwater Vehicle using PMM, oblique towing, and rotating arm tests. They employed dynamic and sliding mesh approaches, utilizing RANS and unsteady RANS equations, and validated the simulation results with experimental data, obtaining comprehensive coefficient values.

This study analyses the hydrodynamic performance of underwater vehicles by obtaining CFD-based rotational derivative hydrodynamic coefficients. The underwater vehicle used as the research object is a development Hybrid Remotely Operated Vehicle (HROV) model from the Digital Ship Technology Laboratory, Department of Naval Architecture, Institut Teknologi Sepuluh Nopember named UUV Segara Nauta (SN-01). The test was conducted virtually using CFD, applying a captive model test through a rotating arm test with radius variations and angular velocities. Determining the hydrodynamic coefficients of the underwater vehicle begins with solving the hydrodynamic forces and moments on the model in horizontal plane with three degrees of freedom (surge, yaw, and sway). The results are subsequently converted into nondimensional values, and hydrodynamic coefficients are determined using a linear regression approach.

2. Methodology

2.1 Coordinate system

The coordinate system adopted is the body-fixed coordinate system. In Figure 1, the body-fixed is located at the G-*xyz* coordinate right at the centre of gravity of the model while moving steady turn with respect to the O-*XYZ* coordinate as the global coordinate. The *x*, *y* and *z* axes define values for the forward direction, starboard direction, and downward direction, respectively. The body-fixed coordinates move in a steady turn rotation of radius R with angular velocity Ω. The use of a non-inertial reference frame introduces the effects of Coriolis and centrifugal forces in the momentum equation [10]. These forces are perpendicular to the velocity vector so they can act to change the direction of motion but not the kinetic energy of the flow.

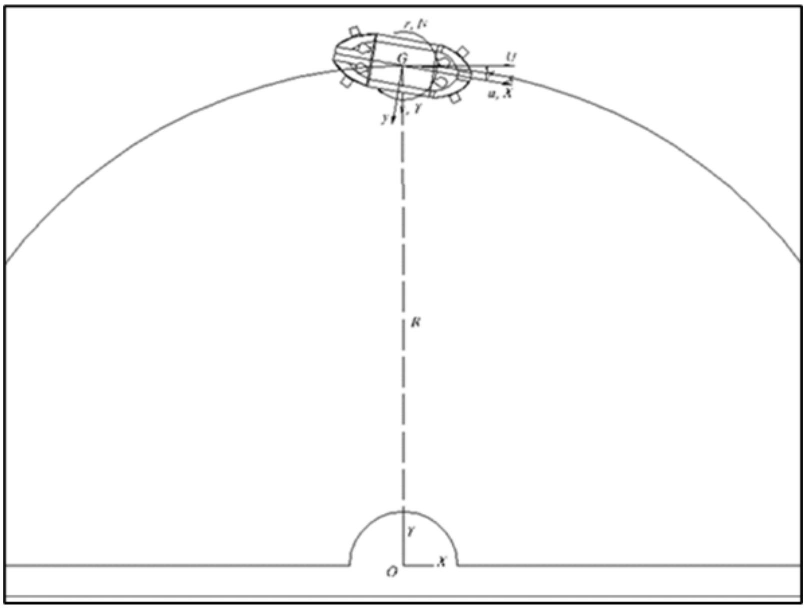

Figure 1. Coordinate system for rotational reference frame in the horizontal plane.

In a non-inertial frame of reference, it is essential to account for additional apparent forces, including the centrifugal and Coriolis forces. The centrifugal force acts radially outward from the axis of rotation, while the Coriolis force induces deflection in the path of moving objects relative to the rotating frame. These fictitious forces arise due to the acceleration of the reference frame and are crucial for accurate motion analysis. The forces will be incorporated as momentum source terms through the implementation of a User-Defined Function (UDF). In the horizontal plane, the source terms are specifically formulated to account for the effects of the rotating reference frame. The centrifugal force is proportional to the radial distance and the square of the angular velocity, while the Coriolis force is dependent on the velocity of the fluid and the angular velocity of the reference frame. By including these source terms, the simulation more accurately reflects the dynamics of the underwater vehicle in a rotating environment, enhancing the precision of the hydrodynamic performance analysis [7].

2.2 Parameter and equation motions

The resulting motion parameters include linear velocity U and angular velocity Ω. In body-fixed coordinates, the linear velocity U can be decomposed into three components: the longitudinal velocity u along the x-axis, the lateral velocity v along the y-axis, and the vertical velocity w along the z-axis. The same principle applies to the angular velocities Ω consisting of the roll angular velocity p about the x-axis, the pitch angular velocity q about the y-axis, and the yaw angular velocity r about the z-axis. For motion in the horizontal plane, it is adequate to consider the surge (longitudinal velocity u), sway (lateral velocity v), and yaw (angular velocity r).

The equations of motion of an underwater vehicle model for horizontal plane solved at specific degrees of freedom are described by the following notation [10, 11].

$$X = m[\dot{u} - vr + wq - x_G(q^2 + r^2) + y_G(pq - \dot{r}) + z_G(pr + \dot{q})] \quad (1)$$

$$Y = m[\dot{v} - wp + ur + x_G(qp + \dot{r}) - y_G(r^2 + p^2) + z_G(qr - \dot{p})] \quad (2)$$

$$N = I_z\dot{r} + (I_y - I_x)pq + m[x_G(\dot{v} - wp + ur) - y_G(\dot{u} - vr + wq)] \quad (3)$$

The model simulation measures the forces and moments acting on the vehicle body at the center of gravity (CG), which aligns with the centerline of the model. These forces include the longitudinal force X along the *x-axis* and the lateral force Y along the y-axis. The yaw moment considered is the yaw moment N around the *z-axis*. The hydrodynamic coefficients are derived from the total sum of hydrodynamic forces, external forces, and thrust forces. However, this study focuses solely on the hydrodynamic damping obtained from the simulation. Additionally, the model's motion is affected by the drift angle in the horizontal plane.

By conducting the rotating arm test, the model was manoeuvered to turn toward the starboard, tracing a circular path. This allowed for the determination of the hydrodynamic coefficients Y_r and N_r resulting from the rotational derivatives. The hydrodynamic coefficient X_r, influenced by rotational derivatives, are zero due to the vertical symmetry of the model. The linear velocity relation of the rotating model is defined by:

$$U = Rr \quad (4)$$

Where R is the radius of rotation and r is the angular velocity in rad/s. To determine the yaw rates r', which are nondimensional values representing angular velocity with respect to the z-axis, the following equation is provided.

$$r' = \frac{rL}{U} \quad (5)$$

The hydrodynamic coefficients are nondimensional quantities of the forces and moments obtained [12]. The process of nondimensionalizing these values is done as referring to (2).

$$X' = \frac{X}{\frac{1}{2}\rho L^2 U^2}; \quad Y' = \frac{Y}{\frac{1}{2}\rho L^2 U^2}; \quad N' = \frac{N}{\frac{1}{2}\rho L^3 U^2} \quad (6)$$

2.3 3D Model simplification

The model geometry is the Segara Nauta (SN-01) model, as shown in Figure 2. This model was developed at the Digital Ship Technology (TKD) Laboratory, Department of Naval Architecture, Institut Teknologi Sepuluh Nopember, featuring a hydrodynamic and modular fish line design [13]. The SN-01 has an overall length of 1.155 meters and can operate at depths of up to approximately 100 meters. Detailed specifications of the Segara Nauta SN-01 are provided in Table 1.

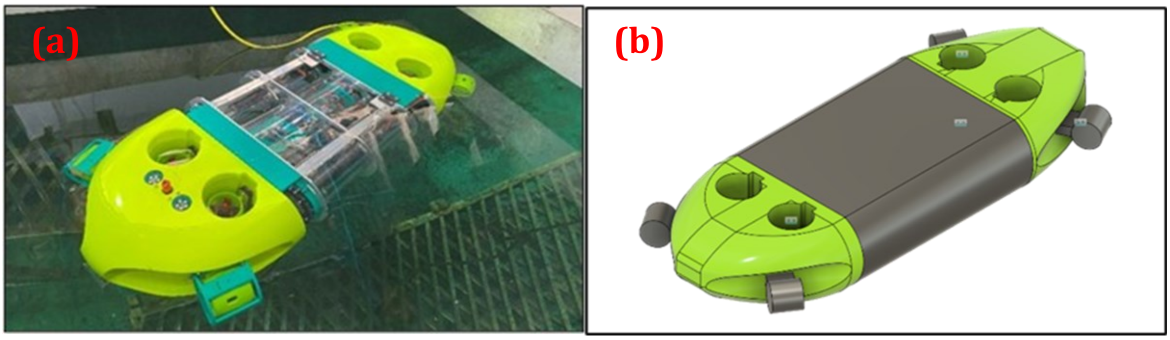

Figure 2. The test model used from the development of the TKD Laboratory FTK-ITS is named Segara Nauta (SN-01) (a); and its simplification model (b).

Table 1. Model specification of UUV SN-01.

Description	Symbol	Value	Unit
Length Overall	L_{OA}	1.155	m
Height	H	0.185	m
Breadth	B	0.450	m
Wetted Surface Area	S_{WA}	1.343	m^2
Center of Gravity	CG	0.582	m from fore

3. CFD Simulation

3.1 Simulation domain setup

The simulation domain is designed to represent the flow around the Segara Nauta (SN-01) model and is solved numerically. Proper domain selection is crucial to accurately depict how the model's shape affects the flow and to prevent boundary effects on the flow [14]. For the rotating arm test, the simulation domain is a half-cylinder, representing the shape of the rotating arm tank and experimental procedure that prevent the model from re-entering its generated flow. The half-cylindrical domain shape was selected to facilitate the clear definition of the flow's inlet and outlet, preventing any overlap that might occur in a full cylindrical domain. The simulation model is positioned at a specific radius (0, R) from the center of the simulation domain (0,0).

The simulation domain, created and discretized with a tetrahedral mesh, features a boundary layer value y^+ of 1 without a wall function. Tetrahedral mesh effectively captures the complex geometry of the model and the simulation domain; however, this comes at the cost of generating a significantly large number of elements. The simulation domain was designed in accordance with ITTC-2014 guidelines, which recommend positioning the boundaries at least one characteristic length L away from the geometry [15]. The boundaries in this simulation were defined by dividing the domain into six faces: the inlet, outlet, and walls [6]. The inlet, located in the positive *xz*-plane, is specified as inlet velocity with input angular velocity value of Ω. The outlet, in the negative *xz*-plane, uses a pressure outlet with default input to facilitate pressure-velocity coupling in RANS solving. The inner, outer, upper, and lower cylinder covers of the wall domain are specified as free-slip, while the wall model itself is specified as no-slip. The fore section of the model faces the positive *x*-axis, and the flow is generated in a circular pattern using a user-defined function (UDF).

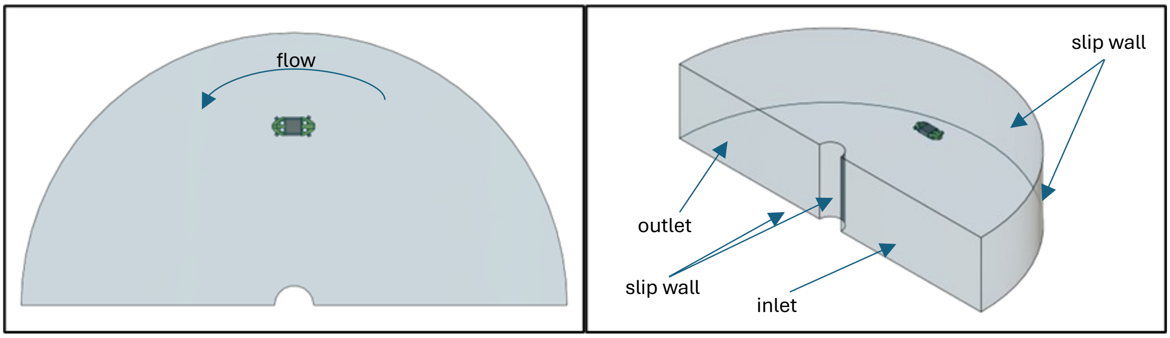

Figure 3. Schematics and simulation domain for the rotating arm test simulation.

3.2 Solver setup for rotating arm

In the steady-state simulation, the solver is configured as pressure-based and utilizes the $k - \omega$ SST turbulence model. This choice is based on the common practice of using a turbulence model to improve the accuracy of velocity profile analysis around the model without the need for wall functions. However, in some cases, the turbulence model alone may be sufficient for the simulation [6]. Within the cell zone conditions, a User-Defined Function (UDF) is employed to introduce source terms to the *x*-axis and *y*-axis momentum equations. The simulation employs the SIMPLE (Semi-Implicit Method for Pressure-Linked Equations) algorithm, which iteratively solves each variable to achieve convergence. Furthermore, the second-order upwind scheme is applied, offering enhanced result accuracy compared to the first-order upwind scheme. This approach ensures precise modeling of the fluid dynamics and turbulence characteristics within the simulation.

The test variations were conducted by altering the radius between the center of gravity (CG) of the model and the central point of the coordinate system, which is situated at the center of the simulation domain. The application of the captive model test adheres to the ITTC-2021 guidelines for rotating arm testing standards and parameters [4]. These variations, detailed in Table 2, aim to investigate the influence of different radial positions on the resulting forces and moments exerted on the model. The simulation results offer detailed data on the forces and moments acting on the model, particularly when it is subjected to rotational and lateral motion. This allows for a thorough analysis of the effects of radial displacement within the simulation domain.

Table 2. Model specification of UUV SN-01.

Linear velocity U (m/s)	Radius R (m)	Angular velocity Ω (rad/s)	Drift angle β
	20.000	0.12	
	15.000	0.16	
2.376	12.000	0.20	-12° s/d 12°, $\Delta\beta$ = 4°
	10.000	0.24	
	8.571	0.28	

3.3 Grid convergence index

To estimate the uncertainty of the simulation results, it is essential to perform a Grid Convergence Index (GCI) analysis. The GCI offers a systematic approach to quantify the error rate and assess the convergence of the simulation. This method involves evaluating three distinct mesh levels: Coarse, Medium, and Fine. Each mesh level is analyzed to determine the degree of numerical error and ensure that the solution is converging appropriately. The input data for this analysis are presented in Table 3, providing a basis for calculating the GCI and thereby validating the accuracy and reliability of the simulation results [16, 17].

Table 3. Detail inputs for Grid Convergence Index calculation.

Parameter	Fine (1)	Medium (2)	Coarse (3)
Surface mesh range (mm)	32 – 256	48 – 384	64 – 512
Total cell count	15,600,325	6,868,429	4,000,493
Dimensionless Y' ($\times 10^4$)	11.785	11.648	10.473

For the UUV SN-01 model, the Grid Convergence Index (GCI) procedure, as detailed in Table 4, was applied to assess the accuracy of the hydrodynamic coefficient calculations. The extrapolated value for the sway force coefficient (Y') was found to be 1.17% for the fine mesh quality level and 10.08% for the coarse mesh quality level. This indicates that the error estimation for the fine mesh is significantly lower, with an approximate relative error of 1.17% and an extrapolated relative error of 0.26%.

Additionally, incorporating a safety factor of 1.25 in the GCI calculation resulted in GCI values of 0.33% for the fine mesh level (GCI_{21}) and 1.04% for the coarse mesh level (GCI_{32}). These results demonstrate the reliability and precision of the simulation data [17]. The final estimated value of Y' is 11.816 with an uncertainty of 0.33%, underscoring the robustness of the fine mesh simulations and the effectiveness of the GCI methodology in ensuring the accuracy of the hydrodynamic coefficients for the UUV SN-01 model.

Table 4. Grid Convergence Index calculation.

Calculation	Symbol	Value
Refinement ratio	$r_i = r_{21} = r_{32}$	1.3
Difference of estimation	$\varepsilon_i = \varepsilon_{21} = \varepsilon_{32}$	$\varepsilon_{21} = -0.138$ $\varepsilon_{32} = -1.174$
Convergence ratio	R_i	0.117 ($Monotonic\ Convergence$)
Order of accuracy	p	9.4
Extrapolation	Y'^{i}_{ext}	$Y'^{21}_{ext} = 11.816$ $Y'^{32}_{ext} = 11.744$
Error estimation: Approximate relative error	e^i_a	$e^{21}_a = 1.17\%$ $e^{32}_a = 10.08\%$
Error estimation: Extrapolated relative error	e^i_{ext}	$e^{21}_{ext} = 0.26\%$ $e^{32}_{ext} = 0.82\%$
Factor of safety	F_s	1.25
Grid Convergence Index	GCI_i	$GCI_{21} = 0.33\%$ $GCI_{32} = 1.04\%$

4. Results and Discussion

4.1 Nondimensional force and moment

The results obtained for the UUV SN-01 model show that the sway force coefficient (Y') and yaw moment coefficient (N') increases as the yaw rates decreases, as shown in Figure 4. This aligns with Equation (5), where lower yaw rates suggest a decrease in the turning radius experienced by the model, while the model's characteristic length and linear velocity remain constant. The yaw rates (r') plays a significant role in the model's motion when assuming a circular turn. A high angular velocity at a low turning radius causes greater lateral forces due to centrifugal force, which acts as a reactive force to maintain the turning path. Consequently, during the design stage, it is crucial to consider the minimum turning radius while maintaining speed, as well as to ensure robust model design and controls to counteract the large drag forces experienced. Beside that, this trend indicates that larger drift angles result in increased lateral forces on the model due to a wider surface being exposed to the flow compared to the model's fore, which is designed to be more hydrodynamic.

Similarly, the yaw moment coefficient (N') exhibits a trend comparable to the sway force coefficient (Y'). The yaw moment coefficient (N'), related to the z-axis, impacts the rotational behavior of the model, where the moment experienced increases with higher drift angles. Notably, the slope of the N' curve is slightly steeper than that of the Y' curve, indicating a greater responsiveness of the yaw moment to changes in drift angle. This suggests that the yaw moment has a more significant influence on the model's drift angle, necessitating careful consideration in the design and control stages to ensure optimal manoeuvering performance, particularly in maintaining yaw motion.

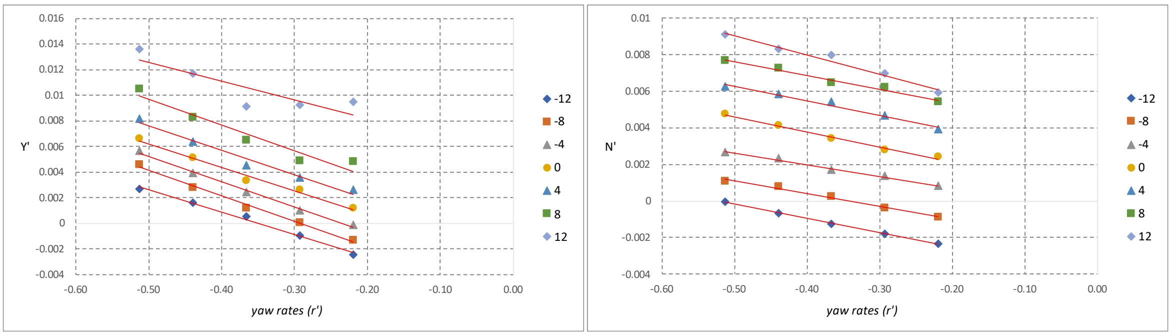

Figure 4. Force Coefficient Y' versus Yaw Rate Function r' (a) and Moment Coefficient N' versus Yaw Rate Function r' (b).

Figure 5 illustrates the pressure contours, revealing a higher-pressure gradient at the outer wall compared to the inner wall due to the centrifugal force in the rotational reference frame, consistent with the applied User-Defined Function (UDF). This pressure distribution highlights how the variation in drift angle significantly impacts flow separation, particularly at the aft and thruster sections of the model. As the drift angle increases, the separation point shifts, affecting the overall hydrodynamic performance. This analysis simulates a circular path with a constant radius, providing insights into the model's behaviour under these conditions. Additionally, variations in drift angle and radius were systematically examined to derive the corresponding force and moment values, enhancing the understanding of the model's dynamics. These findings are crucial for optimizing the design and control strategies of the UUV SN-01, ensuring robust performance in various operational scenarios.

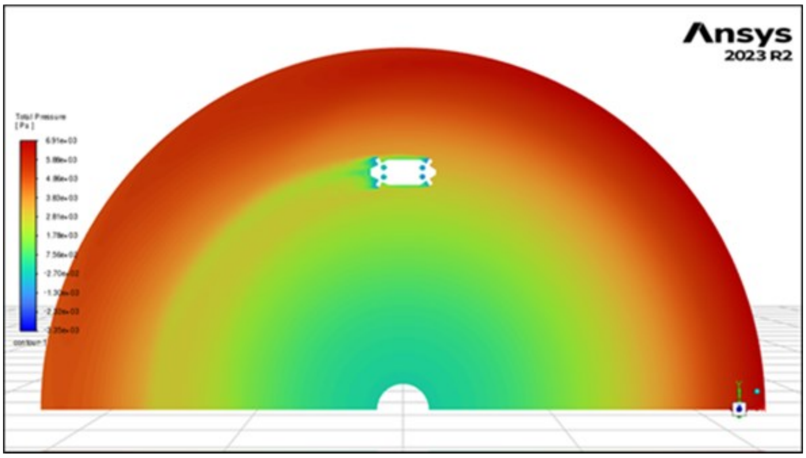

Figure 5. Pressure contour of UUV SN-01.

4.2 Hydrodynamic coefficients

The calculation of hydrodynamic coefficients involves using linear regression, where these coefficients are estimated from the force and moment values obtained through simulations. In this process, the known coefficient values are treated as response variables, while the

IOP Conf. Series: Earth and Environmental Science **1461** (2025) 012037 doi:10.1088/1755-1315/1461/1/012037

nondimensional values of the motion components serve as regressor variables. By performing regression analysis on these variables, the relationship between the response and regressor variables is determined, with the slope of the regression model representing the hydrodynamic coefficient. To accurately determine the magnitude of these coefficients, it is essential to first convert the force and moment values into nondimensional forms, as outlined in equation (6). The calculation is shown in Figure 6.

Table 5. Hydrodynamic coefficients for rotary derivative.

Coefficient	Value × 10^3
Y'_r	-14.441
N'_r	-6.841

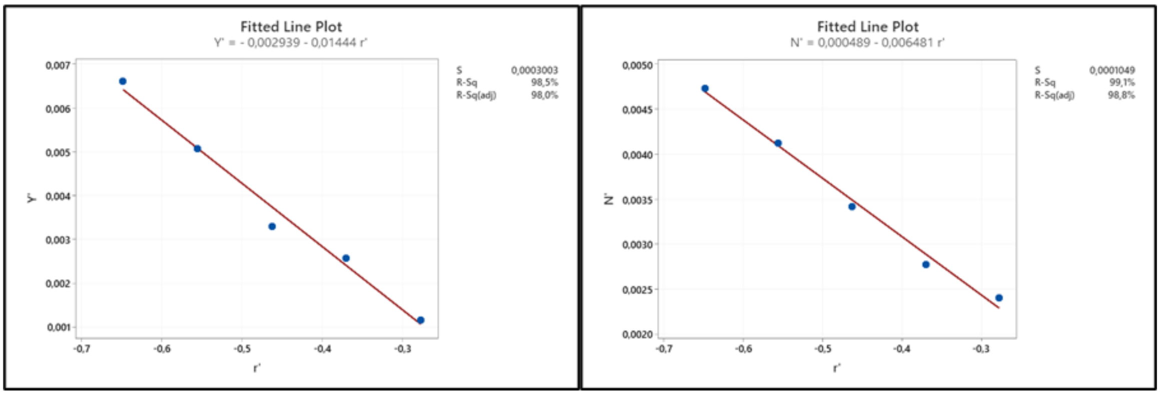

Figure 6. Linear regression function of yaw rates (r'): (a) Force Y' and (b) Moment N'.

5. Conclusion

The application of a virtual captive model test using CFD with rotating arm testing on the UUV SN-01 can be achieved by creating a simulation domain that mimics the actual test pool environment. In these simulations, variations in radius distance and drift angle were applied to the UUV SN-01 model. The resulting forces and moments from these simulations were then converted into nondimensional values for further analysis.

The hydrodynamic coefficients of the UUV, particularly those related to sway and yaw motion due to yaw rates (r') under steady conditions, can be derived from the CFD simulation results. This is accomplished through linear regression analysis, where the nondimensional values of forces and moments are regressed against the nondimensional values of the yaw rates (r') component. This approach allows for a detailed characterization of the UUV's hydrodynamic behaviour.

The CFD simulations revealed that the UUV SN-01 model exhibits a high sensitivity to changes in drift angle and yaw rate, leading to enhanced manoeuvrability. However, this increased sensitivity also results in greater instability in upper control, making it more challenging to maintain stable operation in varying underwater conditions. These findings underscore the need for careful consideration of control strategies to manage the vehicle's responsiveness while ensuring stability in the dynamic underwater environment.

Acknowledgments

This work was supported by the Institut Teknologi Sepuluh Nopember scientific research funding (No. 1209/PKS/ITS/2024).

References

[1] G. Dubbioso, R. Broglia, and S. Zaghi, "CFD analysis of turning abilities of a submarine model," *Ocean Eng.*, vol. 129, no. November 2016, pp. 459–479, 2017, doi: 10.1016/j.oceaneng.2016.10.046.
[2] S. Abdel-Latif, M. Abdel-Geliel, and E. Eldin Zakzouk, "Simulation of ship maneuvering behavior based on the modular mathematical model," *2013 21st Mediterr. Conf. Control Autom. MED 2013 - Conf. Proc.*, pp. 94–99, 2013, doi: 10.1109/MED.2013.6608704.
[3] Y. A. Hermawan and Y. Furukawa, "Coupled three-dimensional dynamics model of multi-component mooring line for motion analysis of floating offshore structure," *Ocean Eng.*, vol. 200, p. 106928, 2020, doi: 10.1016/j.oceaneng.2020.106928.
[4] ITTC, "ITTC - Recommended Procedures and Guidelines: Captive Model Test," *Int. Towing Tank Conf.*, pp. 1–20, 2021.
[5] P. Cardenas and E. A. De Barros, "Estimation of AUV Hydrodynamic Coefficients Using Analytical and System Identification Approaches," *IEEE J. Ocean. Eng.*, vol. 45, no. 4, pp. 1157–1176, 2020, doi: 10.1109/JOE.2019.2930421.
[6] S. Toxopeus *et al.*, "Collaborative CFD Exercise for a Submarine in a Steady Turn," in *Volume 5: Ocean Engineering; CFD and VIV*, Jul. 2012, pp. 761–772, doi: 10.1115/OMAE2012-83573.
[7] L. S. Cao, J. Zhu, and G. H. Zeng, "Numerical Simulation of Oblique Towing Tests and Rotating Arm Tests for a Submarine Model in Same Grid Topology," *Adv. Mater. Res.*, vol. 1083, no. November, pp. 190–196, 2015, doi: 10.4028/www.scientific.net/amr.1083.190.
[8] S. Tang, T. Ura, T. Nakatani, B. Thornton, and T. Jiang, "Estimation of the hydrodynamic coefficients of the complex-shaped autonomous underwater vehicle TUNA-SAND," *J. Mar. Sci. Technol.*, vol. 14, no. 3, pp. 373–386, Sep. 2009, doi: 10.1007/s00773-009-0055-4.
[9] L. Hong, X. Wang, D. Zhang, and H. Xu, "Numerical Study on Hydrodynamic Coefficient Estimation of an Underactuated Underwater Vehicle," *J. Mar. Sci. Eng.*, vol. 10, no. 8, p. 1049, Jul. 2022, doi: 10.3390/jmse10081049.
[10] O. M. Faltinsen, *Hydrodynamics of High-Speed Marine Vehicles*, vol. 9780521845. New York, USA: Cambridge University Press, 2006.
[11] T. I. Fossen, *Guidance and control of ocean vehicles*. Norway: John Wiley & Sons, 1994.
[12] J. Feldman, "DTNSRDC Revised Standarrd Submarine Equations of Motion," Bethesda, MD, 1979.
[13] K. R. Ramadhani, "Studi dan Rancang Bangun Unmanned Underwater Vehicle (UUV) Untuk Perairan Indonesia," Institut Teknologi Sepuluh Nopember, 2023.
[14] ITTC, "Practical Guidelines for Ship CFD Applications," *ITTC – Recomm. Proced. Guidel. ITTC*, pp. 1–8, 2011.
[15] ITTC, "ITTC – Recommended Procedures and Guidelines - Practical guidelines for ship CFD applications. 7.5-03-02-03 (Revision 01)," *ITTC – Recomm. Proced. Guidel.*, p. 19, 2014, [Online]. Available: https://ittc.info/media/4196/75-03-02-03.pdf.
[16] R. Akbar, I. K. Suastika, and I. K. A. P. Utama, "Numerical Study of Effects of Inhomogeneous Roughness on the Ship Friction Resistance," *BIO Web Conf.*, vol. 89, no. 3, pp. 17–27, 2024, doi: 10.1051/bioconf/20248913001.
[17] ITTC, "Uncertainty analysis in CFD Verification and validation methodology and procedures," *ITTC - Recomm. Proced. Guidel.*, pp. 1–13, 2021.